

## MESOSCOPIC PHYSICS

# $h/e$ oscillations in interlayer transport of delafossites

Carsten Putzke<sup>1\*</sup>, Maja D. Bachmann<sup>2,3</sup>, Philippa McGuinness<sup>2,3</sup>, Elina Zhakina<sup>2</sup>, Veronika Sunko<sup>2,3</sup>, Marcin Konczykowski<sup>4</sup>, Takashi Oka<sup>2,5</sup>, Roderich Moessner<sup>5</sup>, Ady Stern<sup>6</sup>, Markus König<sup>2</sup>, Seunghyun Khim<sup>2</sup>, Andrew P. Mackenzie<sup>2,3\*</sup>, Philip J.W. Moll<sup>1\*</sup>

Microstructures can be carefully designed to reveal the quantum phase of the wave-like nature of electrons in a metal. Here, we report phase-coherent oscillations of out-of-plane magnetoresistance in the layered delafossites PdCoO<sub>2</sub> and PtCoO<sub>2</sub>. The oscillation period is equivalent to that determined by the magnetic flux quantum,  $h/e$ , threading an area defined by the atomic interlayer separation and the sample width, where  $h$  is Planck's constant and  $e$  is the charge of an electron. The phase of the electron wave function appears robust over length scales exceeding 10 micrometers and persisting up to temperatures of  $T > 50$  kelvin. We show that the experimental signal stems from a periodic field modulation of the out-of-plane hopping. These results demonstrate extraordinary single-particle quantum coherence lengths in delafossites.

Electrons in vacuum carry the characteristics of both particles and waves, which has been demonstrated in interference experiments directly probing the phase information (1). In metals, the transport properties are usually well captured by the particle nature of the electron only, as described by the semiclassical Boltzmann equation. The wave-like character is masked by the high density of electrons and their interaction with the ionic lattice, which leads to a loss of the phase information in bulk phenomena. With experimental effort, samples can be fabricated on the mesoscopic length scale over which the phase of the electron is preserved, thus becoming observable in electronic transport. A well-known example is the Aharonov-Bohm effect (ABE) in nanoscopic rings of gold (2, 3), which presents a solid-state analog of the interference experiment by Davisson and Germer (1). Common to these experiments is the creation of an artificial loop enclosing magnetic flux, which acts as a beam splitter.

Here, we report an unexpected robust manifestation of phase coherence intrinsic to the out-of-plane transport in single bars of the ultrapure delafossites PdCoO<sub>2</sub> and PtCoO<sub>2</sub>. These materials are composed of highly con-

ducting Pd/Pt layers separated by CoO<sub>2</sub> layers, resulting in a large transport anisotropy  $\rho_c/\rho_a$  exceeding 1000. The layered triangular crystal lattice leads to an almost hexagonal Fermi surface (FS) (4) with little warping, which has been well characterized by de Haas-van Alphen oscillations (5) and angle-dependent magnetoresistance oscillations (6, 7). These materials are the most conductive oxides known, with an in-plane transport mean free path (mfp) of  $>20$   $\mu\text{m}$  at low temperatures (5, 8, 9).

The strong anisotropy is also reflected in the growth of thin, plate-like crystals, a common property of layered materials. Although mesoscopic quantum phenomena are successfully probed in the plane of quasi-two-dimensional (2D) ultrapure metals, achieving such electrical transport perpendicular to the layers is challenging. We have overcome this difficulty by using focused ion beam (FIB) microstructuring techniques (10). Starting from as-grown crystals, we milled pillars along the  $c$ -axis, thereby restricting the in-plane dimensions to a few micrometers. A typical structure designed for four-point resistivity measurements is shown in Fig. 1A. Because the depth  $d$  and width  $w$  of the pillar are both well below the mfp, the system enters the ballistic transport regime in the plane.

We found an oscillatory magnetoresistance by applying an in-plane magnetic field at low temperatures (Fig. 1B). These oscillations are clearly visible in the raw data ( $\Delta\rho_{osc}/\rho \sim 5\%$ ; Fig. 1). To perform further analysis, we focused on the second derivative of the magnetoresistance (Fig. 1C). The oscillations are periodic in magnetic field and their periodicity scales inversely with the width of the pillars over an order of magnitude, from 1.2 to 12  $\mu\text{m}$  (Fig. 1D).

The observed periodicity matches very well with that expected for a magnetic flux quantum  $\Phi_0 = h/e$ , with the Planck constant  $h$  and electron charge  $e$ , threading through an area  $S$  enclosed by two adjacent Pd/Pt layers and the sample side walls (dashed line in Fig. 1D). This gives an area  $S = w^*c/3$ , where  $c$  denotes the crystallographic unit cell lattice constant (PdCoO<sub>2</sub>: 1.774 nm; PtCoO<sub>2</sub>: 1.781 nm) (11). Owing to the ABC stacking, the unit cell contains three Pd/Pt layers so the relevant height is  $c/3$ . Such oscillations of the magnetoresistance, periodic in  $\Phi_0$ , demonstrate quantum transport of coherent electron waves spanning the width of the entire sample. Oscillations are readily observed in samples as wide as 12  $\mu\text{m}$ , indicating a macroscopic phase preservation in the metal. PdCoO<sub>2</sub> has been shown to have an extremely long ballistic mfp (12), but observation of phase coherence in a high-carrier-density metal over such a long distance is still unexpected. It is particularly noteworthy that no special care had to be taken to decouple the sample from the environment, such as ultralow temperatures or substrate decoupling [all samples are simply attached to a sapphire chip by epoxy glue; see the materials and methods (13)]. Nevertheless, all samples from different crystals showed a highly consistent picture of strong, long-ranged quantum coherence.

So far, we have only considered magnetic fields applied perpendicular to the sample surface. If indeed the oscillation frequency is set by the flux through the area  $S$ , then it would be natural to expect a sinusoidal dependence on the magnetic field angle when rotating within the Pd/Pt layer. The experimental frequency spectrum upon rotation is more complex, with multiple frequencies appearing (Fig. 2). A natural geometric interpretation of the angle dependence is found because of the FS topography of PdCoO<sub>2</sub>. The almost perfect hexagonal FS, in contrast to a circular one, exhibits three preferential directions of electron motion perpendicular to the flat faces of the FS. In real space, this describes three interweaving subsystems of directional electron flow in the plane, each spanning its own area  $S_i$  (where  $i = 1..3$ ; sketched in Fig. 2A). The flux enclosed in each subsystem contributes oscillations of frequency  $|\vec{B} \cdot \vec{S}_i|/\Phi_0$  to the total conduction, leading to three branches in the frequency spectrum offset by  $60^\circ$  from each other. The difference in symmetry between the hexagonal FS and the rectangular sample shape divides the branches into two different types. The samples are cut such that one preferential direction of motion is aligned with a sample side wall. Therefore, one subsystem area is set by the full sample depth, whereas two symmetric branches are related geometrically to the sample width. The aspect ratio

<sup>1</sup>Laboratory of Quantum Materials (QMAT), Institute of Materials, École Polytechnique Fédérale de Lausanne (EPFL), 1015 Lausanne, Switzerland. <sup>2</sup>Max Planck Institute for Chemical Physics of Solids, 01187 Dresden, Germany. <sup>3</sup>School of Physics and Astronomy, University of St. Andrews, St. Andrews KY16 9SS, UK. <sup>4</sup>Laboratoire des Solides Irradiés, CEA/DRF/IRAMIS, École Polytechnique, CNRS, Institut Polytechnique de Paris, 91128 Palaiseau, France. <sup>5</sup>Max Planck Institute for the Physics of Complex Systems, 01187 Dresden, Germany. <sup>6</sup>Weizmann Institute of Science, Department of Condensed Matter Physics, Rehovot 76100, Israel.

\*Corresponding author. Email: carsten.putzke@epfl.ch (C.P.); andy.mackenzie@cpfs.mpg.de (A.P.M.); philip.moll@epfl.ch (P.J.W.M.)

**Fig. 1. Magnetoresistance oscillations periodic in magnetic field.** (A) Experimental setup. (Left) Current is passed along a bar-shaped sample perpendicular to the layered structure. The bars have a width  $w$  and a thickness  $d$ . Magnetic field is applied and rotated within the Pd/Pt layer. (Middle) Scanning electron microscope image of PdCoO<sub>2</sub> microstructure to measure  $c$ -axis resistivity. (Right) Crystal structure of PdCoO<sub>2</sub> and PtCoO<sub>2</sub>. Alternating layers of Pd/Pt and CoO<sub>2</sub> lead to a high anisotropy of the resistivity. The area  $S$  relevant for the  $h/e$  oscillations is spanned by two adjacent Pt/Pd layers. (B) Magnetoresistance of PtCoO<sub>2</sub> and PdCoO<sub>2</sub> at  $T = 2$  K of various sample widths for fields along the  $a$  axis. The apparent difference in the high-field background is caused by a sharp feature in the angle-dependent magnetoresistance when fields are close to parallel with the Pd/Pt layers (7). (C) The second derivative of the resistivity highlights the oscillatory part of the magnetoresistance in (B). Multifrequency components are well explained by small sample misalignment (see Fig. 2). (D) The oscillation period is shown for different sample widths. The sample width dependence shows extraordinary agreement with the oscillation period expected for a single-particle magnetic flux quantum,  $h/e$ , per area  $S = w \cdot c/3$  (as indicated in the panel above).

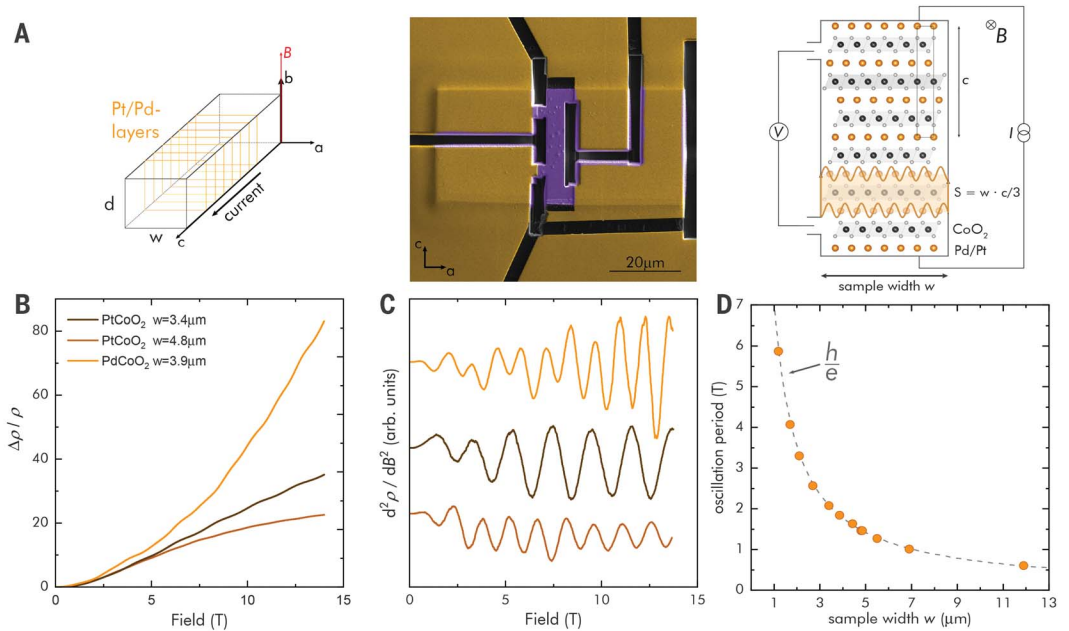
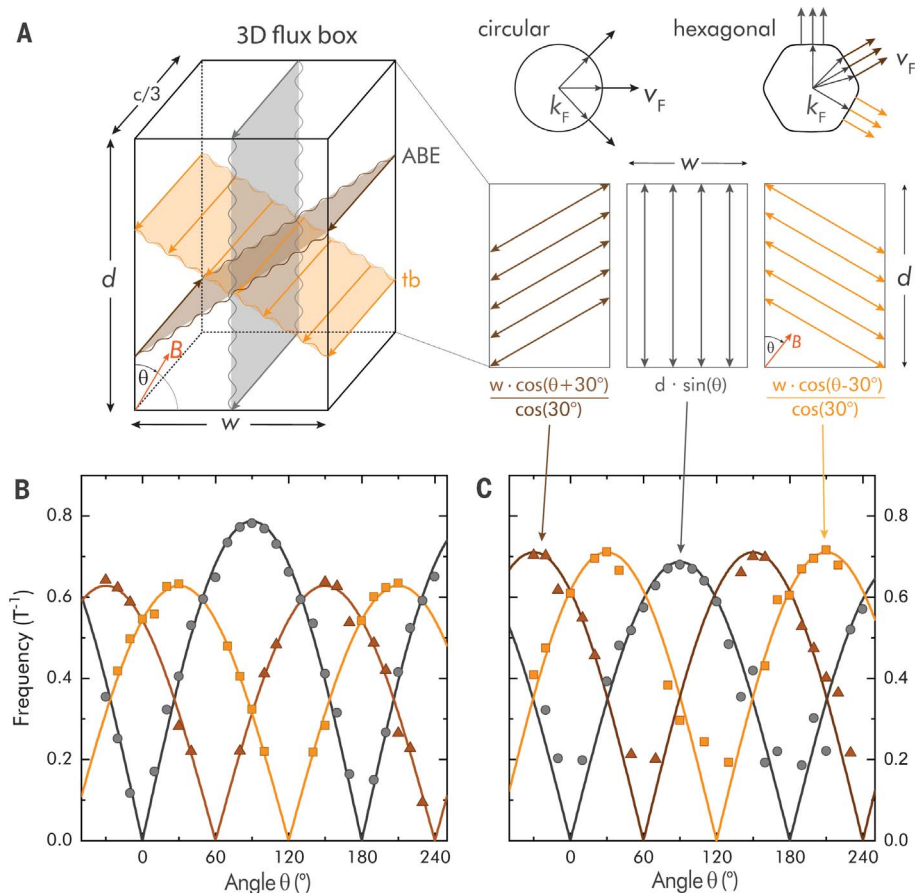


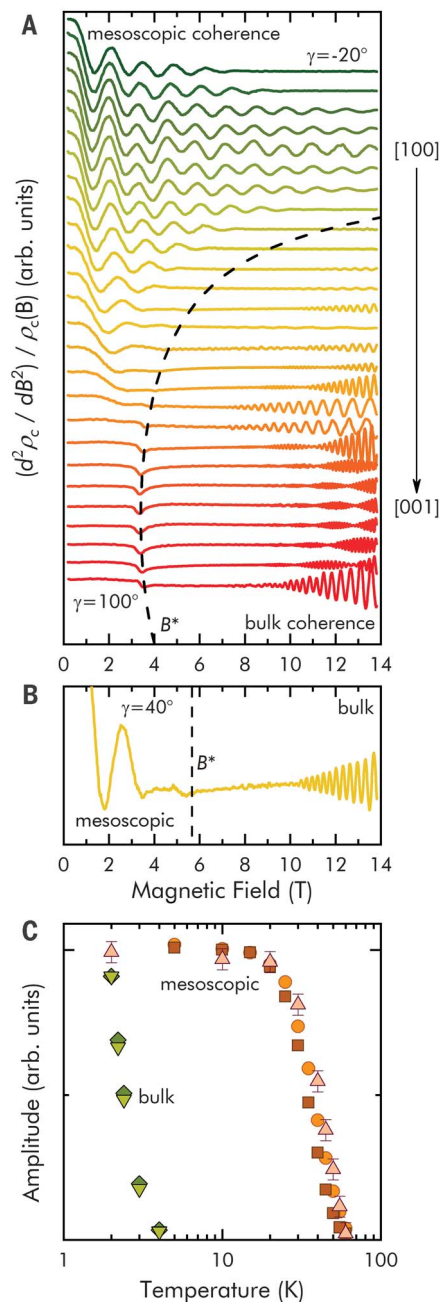
**Fig. 2. Angle dependence of quantum-coherent oscillations.** (A) Pd/PtCoO<sub>2</sub> has almost hexagonal FS's (4, 32). This leads to three preferred directions of motion, unlike the case with a circular FS. The magnetic field is rotated in the planes. The three ballistic paths and their angle-dependent projections on the magnetic field are shown. In rectangular samples, two symmetric branches are set by the sample width and one by the sample thickness  $d$  (see discussion in main text). The left panel illustrates the relevant 3D flux box limited by the sample width, thickness, and two adjacent Pd/Pt layers. This box defines the flux surfaces. The oscillations are periodic in integer flux quanta threading through them. (B and C) Angle dependence of the quantum-coherent oscillations of PdCoO<sub>2</sub> (B) and PtCoO<sub>2</sub> (C). Solid symbols represent the measured data points, and solid lines represent the expectation from the model sketched in (A). (B) shows data from a sample with a  $d/w$  ratio of 1.4, whereas the aspect ratio for the sample in (C) is close to 0.9.



Downloaded from <http://science.sciencemag.org/> on June 13, 2020

**Fig. 3. Angle dependence tilting the field out of the plane.**

**(A)** Second derivative of the magnetoresistance with respect to the magnetic field.  $B$ -periodic oscillations in agreement with Fig. 1 for angle  $\gamma = 0^\circ$  are shown. As the field is tilted out of the Pd layers in  $5^\circ$  steps, the oscillation period is modified as  $1/\cos \gamma$ . At higher tilt angles, the  $B$ -periodic oscillations vanish and SdH oscillations are observed (for a detailed analysis, see fig. S5). The dashed line represents the field  $B^*$  at which the cyclotron diameter coincides with the sample width  $w$ .  $B$ -periodic oscillations are seen over a wide-angle range below  $B^*$ , whereas SdH oscillations only appear above  $B^*$ . The data have been offset proportional to the magnetic field angle. **(B)** Subset of the data in (A) at a magnetic field angle of  $\gamma = 40^\circ$ . At low field, the  $B$ -periodic oscillations are seen, whereas at high field,  $1/B$ -periodic oscillations are observed. **(C)** Mesoscopic oscillation amplitudes extracted from fast Fourier transform (FFT) analysis (see raw data in fig. S4) in the field range from 3 to 12 T and  $\gamma = 0^\circ$  are shown for PtCoO<sub>2</sub> ( $w = 4.8 \mu\text{m}$ , squares;  $w = 2.0 \mu\text{m}$ , circles) and two samples of PdCoO<sub>2</sub> (#1: mfp =  $20 \mu\text{m}$ ,  $w = 3.9 \mu\text{m}$ , diamonds; #2: mfp =  $1 \mu\text{m}$ ,  $w = 1 \mu\text{m}$ , triangles). Despite the large changes of width and mfp, the temperature dependence of the signals from the different samples is very similar and the oscillations can be observed to temperatures of  $>50 \text{ K}$ . By comparison, the temperature dependence of the conventional bulk SdH oscillations ( $\gamma = 90^\circ$ ) is shown for the two main orbits (see fig. S5).



of the cross section is reflected in the relative ratio of the maximum frequency values in the two types of branches. From the in-plane angle dependence, it follows that for the magnetic field aligned with both the sample sides ( $\theta = 0^\circ$  and  $90^\circ$ ), an area  $S_i$  scales with  $w$  or  $d$ , respectively. In Fig. 1D, the data for both angle configurations were combined by denoting the dimension perpendicular to magnetic field as sample width  $w$ .

The period of all field-induced oscillations in quantum objects is expected to be the flux quantum threading through them,  $B_n \cdot S = n\Phi_0$ . Usually, the relevant length scale in me-

tallic systems is set by the magnetic field itself, in the form of the cyclotron radius  $r_c$ , leading to oscillations periodic in  $1/B$  ( $B_n \cdot r_c^2 \propto n\Phi_0$ ). The best known of such  $1/B$  periodic magnetoresistance oscillations are Shubnikov-de Haas (SdH) oscillations (14). Given the 2D nature of the FS in our system, SdH oscillations will not appear for in-plane fields because all orbits are open. However, as the magnetic field is rotated out of the Pd layers, the out-of-plane field induces orbital motion and usual SdH oscillations will appear. This leads to a particularly rich interplay between the different quantum transport regimes as a function of

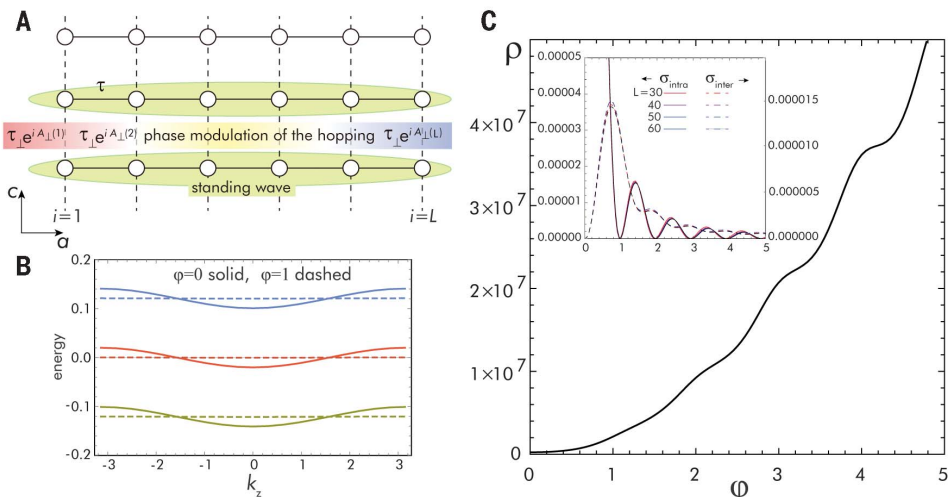
out-of-plane angle  $\gamma$  (Fig. 3). For an in-plane magnetic field ( $\gamma = 0^\circ$ ),  $B$ -periodic oscillations are observed as previously discussed. On tilting the field out of plane, those oscillations are limited to lower magnetic fields and vanish at a field scale  $B^*$  defined by the mesoscopic size of our samples (Fig. 3B).  $B^*$  corresponds to the angle-dependent field scale required to fit a bulk-like cyclotron radius into the pillar, given by the condition of  $2r_c = w$ .  $B^*$  appears as a clear anomaly in the magnetoresistance, delineating a strong negative magnetoresistance above  $B^*$  (fig. S3). Thereby, tilted magnetic fields induce a transition between mesoscopic quantum transport in the low-field regime and bulk-like transport described by Landau levels at sufficiently high fields. This picture is straightforward to understand: Once the in-plane Lorentz force is sufficient to bend a wave front back on itself, it will self-interfere, leading to Landau quantization. This detaches the wave function from the boundary, and thus the Landau levels are entirely bulk like and independent of sample width. This scenario is further supported by the negative magnetoresistance above  $B^*$  (fig. S3), which is caused by the suppression of the dominant boundary scattering in the clean devices owing to bulk-like Landau tubes forming in the core of the pillar. Indeed, above  $B^*$ , conventional SdH oscillations are observed in our samples, which coexist with  $B$ -periodic oscillations in the intermediate angle range (Fig. 3B). The SdH frequencies and effective masses of  $m^* \approx 1.5 m_e$  [PtCoO<sub>2</sub> (5)] and  $1.2 m_e$  [PtCoO<sub>2</sub> (7)] are consistent with work performed on macroscopic crystals, clearly excluding the possibility that the microfabrication has strongly altered the material. The large size of the hexagonal FS leads to high-frequency oscillations around  $F \sim 30 \text{ kT}$  observed in the microstructure. However, resolving such high frequencies requires very slow field sweeps ( $<10 \text{ mT/min}$ ), which are impractical to perform over large field ranges and multiple angles. Therefore, only the slow difference frequency corresponding to the beating of neck and belly frequencies is apparent in Fig. 3; the main frequencies were always observed consistently when sweeping more slowly (fig. S5).

Further insights into the quantum transport arise from a comparison of the transport mfp and the quantum mfp. The quantum coherence length extracted from SdH oscillations is found to be only  $400 \text{ nm}$  (fig. S6), more than an order of magnitude smaller than that observed in the  $B$ -periodic oscillations. Furthermore, the quantum coherence length remains almost unchanged in irradiated samples, whereas the in-plane transport mfp is reduced by more than a factor of 10. It is important to consider that the quantum mfp obtained from a Dingle analysis

**Fig. 4. Transport analysis for the anisotropic Hofstadter model.**

(A) Anisotropic Hofstadter model with tunneling parameters  $\tau_1 = 100\tau_\perp = 1$  as a toy model to study the origin of the  $h/e$  magneto-oscillation shown in Fig. 1. Interlayer transport occurs as an electron in one layer, in an extended standing wave state, tunnels to an adjacent layer. In the presence of a magnetic field, the tunneling matrix element is modulated by a phase factor  $e^{i2\pi\frac{\varphi}{L}j}$  caused by the  $c$ -direction gauge field  $A(j) = 2\pi\frac{\varphi}{L}j$ , where  $\varphi$  is the flux per area between adjacent layers. This model naturally yields an effective interplane bandwidth given by  $2\tau_\perp \text{Re}A(\varphi)$  in the large

$L$  and an anisotropic limit that vanishes for integer values of  $\varphi$ , where the factor  $A(\varphi)$  resembling a diffraction grating effect is explained in the main text. (B) Energy spectrum of the anisotropic Hofstadter model around zero energy for  $L = 51$  showing vanishing bandwidth at  $\varphi = n$  (integer). (C) Resulting calculations of the interlayer resistivity. Full details of the calculation are presented in the materials and methods (13). In the absence of incoherent (e.g., phonon-assisted)



interlayer processes, the resistivity would diverge for integer  $\varphi$  because only the intraband term  $\sigma_{\text{intra}}$  in the Kubo formula contributes (inset). However, for large  $L$ , the level separation shown in (B) becomes smaller than the level broadening from such incoherent processes, motivating the inclusion of interband contributions  $\sigma_{\text{inter}}$  in the calculation for the results shown in (C).

represents an average over the entire FS orbit, whereas the  $B$ -periodic oscillations stem exclusively from the flat sections of the hexagonal FS. A resolution to this conundrum would be a large quantum scattering rate at the corners of the hexagon; evidence of this has been reported previously in an analysis of the Hall effect (15).

$B$ -periodic oscillations in a metal, such as those reported here, arise when a field-independent area  $S$  enters the quantization condition, such that  $B_n \cdot S = n\Phi_0$ . This most notably occurs in samples that are not simply connected geometrically. In these samples, e.g., Aharonov-Bohm rings or cylinders, a physical hole defines the relevant area. Such a physical area is naturally absent in our simply connected, bar-shaped samples. The experimental situation is also far from the so-called ultraquantum limit, at which the magnetic flux per crystalline unit cell is comparable to one flux quantum. This extreme limit requires fields on the order of  $\Phi_0/\text{\AA}^2 \sim 10^5$  T, at which  $B$ -linear oscillations from an atomic-scale flux box might be expected, yet such fields are inaccessible. The few known  $B$ -linear oscillatory phenomena in singly connected solids are semiclassical [Sondheimer resonances (16), Azbel-Kaner cyclotron motion (17), or geometric resonances in the presence of acoustic waves]; rely on a superconducting order parameter to establish macroscopic phase coherence [Fraunhofer interference in Josephson junctions (18)] or exploit artificially introduced nanometric length scales or interference effects in tunneling between parallel quantum wires or wells (19).

None of these can explain our data because the observed  $h/e$  periodicity clearly indicates long-range, single-particle-phase coherence as their origin.

Given the flux quantization condition that we have identified, it is at first sight appealing to invoke a scenario akin to the ABE to account for our data. In this picture, the quasiparticle would encircle the area  $S$  with the Pd/Pt layers resembling the arms of an interferometer. Because the nanoscopic dimensions of the interlayer distance would be combined with the macroscopic sample width, the necessary fields would be scaled to the range accessible in superconducting magnets. Although this would naturally lead to the observed periodicity, this scenario has severe shortcomings. First, the Pd layers are too strongly coupled through the sizable out-of-plane hopping element  $\tau_\perp$  as determined by quantum oscillations ( $\tau_\perp = 1$  eV;  $\tau_\perp = 10$  meV) (8), leading to an infinite number of paths involving a large number of layers. Furthermore, the ABE is most commonly accompanied by a related self-interference effect caused by weak localization called the Altshuler-Aronov-Spivak effect (20), which gives oscillations periodic in  $h/2e$  in metallic rings (2, 3, 21). This, or any other higher-order quantum process involving multiple layers in a stack (2S, 3S, ...), would lead to higher harmonic content of the oscillations, which was not observed experimentally here within the noise level of 1% (fig. S2). A third key feature of our observation is its robustness to temperature (Fig. 3C). The observation of

the ABE in metallic rings was limited to  $<4$  K because of decoherence from various types of interaction with the environment, something that is also a feature of reported ABE experiments on graphene (22). This is in stark contrast to the  $T > 50$  K temperature scale observed here in highly metallic PdCoO<sub>2</sub> and PtCoO<sub>2</sub>. Similar high-temperature quantum coherence has been seen in bismuth nanowires (23), topological nanoribbons (24, 25), quantum dots (26), carbon nanotubes (27), and  $1/B$  superlattice oscillations in graphene (28), but the key to its observation was the small length scale involved in those nanoscale systems. This is not surprising in light of the calculation presented in the materials and methods (13), in which we show that even if we impose a far larger  $\tau_\perp$  at the sample edge than in the bulk, an ABE-style calculation predicts an experimental signal with an amplitude dying out as  $1/w$ . For our situation, this signal would be unresolvable.

Because the mfp decreases with increasing temperature, one would expect the  $h/e$  oscillations to persist up to higher temperatures for samples with smaller width  $w$ . By contrast, the onset temperature appears independent of sample width, which suggests that the upper temperature limit is not set by the mfp in the sample. To further probe this observation, we performed an additional set of measurements on a device in which the mfp had been reduced by a factor of 20 to  $1 \mu\text{m}$  by the introduction of point defects created by 2.5 MeV of electron irradiation (29). Oscillations were unresolvable when the device width was  $8 \mu\text{m}$

and reappeared when it was narrowed to 1  $\mu\text{m}$  (fig. S7), consistent with the expectation that the mfp must be on the order of the sample width or larger for the signal to be seen. Unexpectedly, the temperature dependence of the oscillations in the disordered device was the same as that in the cleaner devices within experimental error (Fig. 3C). This strongly suggests that if the zero temperature in-plane mfp exceeds the sample width, then the oscillatory signal persists until  $k_B T$  (where  $k_B$  is the Boltzmann constant) becomes a substantial fraction of  $\tau_{\perp}$  despite the mfp becoming smaller than the device width at elevated temperatures.

This leads to a different scenario in which the purity of the experimental system plays an intriguing dual role. First, it provides a wave function with full phase coherence across the length of the  $ab$  plane. Second, the microscopically regular structure of the essentially perfect delafossite crystals gives rise to a periodic array of tunneling paths between the layers in the  $c$  direction.

In our picture, a phase coherent wave in the  $ab$  plane is transmitted to an adjacent plane with tunneling matrix elements  $\tau_{\perp} \ll \tau_{\parallel}$  in each unit cell of the lattice. For a field applied along  $b$ , the phase of the tunneling matrix elements at site  $j = 1..L$  is modulated by a factor  $e^{i 2 \pi \frac{\varphi}{L} j}$ . The field strength is written such that there is a total flux  $\varphi = |\vec{B} \cdot \vec{S}_i| / \Phi_0$  per layer across the system of width  $L$  ( $= w/\text{lattice constant}$ ) in the  $a$  direction. Summing the resulting series yields the following equation:

$$A(\varphi) = \sum_{j=1}^L e^{i 2 \pi \frac{\varphi}{L} j} = \frac{1 - e^{i 2 \pi \varphi}}{e^{-i 2 \pi \frac{\varphi}{L}} - 1}$$

The reader will recognize this as equivalent to the far-field diffraction pattern from a diffraction grating of finite width  $L$  illuminated by a coherent light field. The finite width of such a grating is modeled by multiplying the transmission function of an infinite grating with a boxcar function (also known as a top hat function),  $\text{rect}(L)$ . Invoking the convolution theorem of the Fourier transformation, its far-field diffraction pattern becomes convolved with the Fourier transform of  $\text{rect}(L)$ , namely  $\text{sinc}(L)$ . This is, we believe, the key physics behind our observation because this convolution gives rapid oscillations at a frequency that depends on  $L$  but with a relative amplitude from one oscillation to the next that is approximately  $L$  independent. In our experiment, the applied field is small, such that  $\varphi/L \ll 1$ , and we observed only the first few oscillations of the sinc function.

Reflecting this intuitive picture, we performed a transport calculation using the finite system Kubo formula (30–32) in the anisotropic Hofstadter model, which is summa-

rized in Fig. 4 and presented in detail in the materials and methods. The calculation reproduces the qualitative experimental signal very well, with the expected sinc function clearly evident in Fig. 4C. It also provides a further key insight: The bandwidth for interplane transport (Fig. 4B) is seen to be modulated by the field, even vanishing for special fields at which  $\varphi$  is an integer, even though the bare-hopping  $\tau_{\perp}$  remains unchanged.

The extremely anisotropic nature of the area pierced by the flux quantum—truly microscopic in one direction, almost macroscopic in the other—extends the experimentally accessible regime of the famous Hofstadter Hamiltonian to a region in which the hopping terms in the plaquette are highly anisotropic.

A natural question is why these oscillations, seen so clearly in our raw data, have not been observed before. The answer is that, in addition to the rarity of crystalline perfection at the level found in the delafossites, only recent technological advances have enabled experimental investigations of this regime (10). The technical key to this observation is to reduce  $w$  to a few micrometers, as well as to shape the sample cross section into an ideal rectangle by FIB. This acts as a magnifying glass that allows us to venture deeper into the mechanism behind coherent interlayer transport.

We believe that the observations and analysis reported here will stimulate further experimental, theoretical, and technological research. The framework that we have presented for understanding the data invites refinement, and a similar physical picture might be developed from slightly different starting viewpoints. It may also be possible to extend the experiments to other high-purity layered compounds such as the ruthenates. Furthermore, the evolution of the signal could be studied by fabricating bilayer and few-layer thin films. Such thin films may also be used to explore technological possibilities. As quantum coherence emerges as its own subject in technology, it will be interesting to explore whether applications can exploit the rare macroscopic, single-particle phase coherence in the delafossites.

#### REFERENCES AND NOTES

- C. J. Davisson, L. H. Germer, *Proc. Natl. Acad. Sci. U.S.A.* **14**, 317–322 (1928).
- V. Chandrasekhar, M. J. Rooks, S. Wind, D. E. Probe, *Phys. Rev. Lett.* **55**, 1610–1613 (1985).
- R. A. Webb, S. Washburn, C. P. Umbach, R. B. Laibowitz, *Phys. Rev. Lett.* **54**, 2696–2699 (1985).
- H. J. Noh *et al.*, *Phys. Rev. Lett.* **102**, 256404 (2009).
- C. W. Hicks *et al.*, *Phys. Rev. Lett.* **109**, 116401 (2012).
- J. C. A. Prentice, A. I. Coldea, *Phys. Rev. B* **93**, 245105 (2016).
- N. Kikugawa *et al.*, *Nat. Commun.* **7**, 10903 (2016).
- H. Takatsu *et al.*, *Phys. Rev. Lett.* **111**, 056601 (2013).
- A. P. Mackenzie, *Rep. Prog. Phys.* **80**, 032501 (2017).
- P. J. W. Moll, *Annu. Rev. Condens. Matter Phys.* **9**, 147–162 (2018).
- M. Tanaka, M. Hasegawa, H. Takei, *J. Cryst. Growth* **173**, 440–445 (1997).
- M. D. Bachmann *et al.*, *Nat. Commun.* **10**, 5081 (2019).
- See the supplementary materials.
- D. Shoenberg, *Magnetic Oscillations in Metals* (Cambridge Univ. Press, 1984).
- N. Nandi *et al.*, *npj Quantum Mater* **3**, 66 (2018).
- E. H. Sondheimer, *Phys. Rev.* **80**, 401–406 (1950).
- M. I. Azbel, E. A. Kaner, *Sov. Phys. JETP* **30**, 811 (1956).
- S. Ooi, T. Mochiku, K. Hirata, *Phys. Rev. Lett.* **89**, 247002 (2002).
- S. Datta *et al.*, *Phys. Rev. Lett.* **55**, 2344–2347 (1985).
- B. L. Altshuler, A. G. Aronov, B. Z. Spivak, *P. Zh. Eksp. Teor. Fiz.* **33**, 101 (1981).
- C. P. Umbach, S. Washburn, R. B. Laibowitz, R. A. Webb, *Phys. Rev. B* **30**, 4048–4051 (1984).
- S. Russo *et al.*, *Phys. Rev. B Condens. Matter Mater. Phys.* **77**, 085413 (2008).
- A. Nikolaeva, D. Gitsu, L. Konopko, M. J. Graf, T. E. Huber, *Phys. Rev. B* **77**, 17–19 (2008).
- H. Peng *et al.*, *Nat. Mater.* **9**, 225–229 (2010).
- L. X. Wang, C. Z. Li, D. P. Yu, Z. M. Liao, *Nat. Commun.* **7**, 10769 (2016).
- I. R. Sellers, V. R. Whiteside, I. L. Kuskovsky, A. O. Govorov, B. D. McCombe, *Phys. Rev. Lett.* **100**, 136405 (2008).
- A. Bachtold *et al.*, *Nature* **397**, 673–675 (1999).
- R. Krishna Kumar *et al.*, *Science* **357**, 181–184 (2017).
- V. Sunko *et al.*, *Phys. Rev. X* **10**, 021018 (2020).
- G. Czycholl, B. Kramer, *Solid State Commun.* **32**, 945–951 (1979).
- Y. Imry, N. S. Shiren, *Phys. Rev. B* **33**, 7992–7997 (1986).
- D. J. Thouless, S. Kirkpatrick, *J. Phys. C Solid State Phys.* **14**, 235–245 (1981).
- C. Putzke *et al.*, Data for:  $h/e$  oscillations in interlayer transport of delafossites, Zenodo (2020); <https://doi.org/10.5281/zenodo.3725930>.

#### ACKNOWLEDGMENTS

We thank B. Ramshaw, R. Ilan, M. Fischer, A. Morpurgo, J. Schmalian, and L. Forro for helpful discussions. **Funding:** This project was funded by the European Research Council (ERC) under the European Union's Horizon 2020 research and innovation program (grant no. 715730, MiTopMat) and also was supported by the Max Planck Society. A.P.M. and R.M. acknowledge support from the Würzburg-Dresden Cluster of Excellence on Complexity and Topology in Quantum Matter (EXC 2147). M.D.B., P.M., and V.S. acknowledge studentship funding from the EPSRC under grant no. EP/L015110/1. A.S. was supported by the Israel Science Foundation, the European Research Council (Project LEGOTOP), and the DFG through project no. CRC-183. M.K. acknowledges support from the SIRIUS irradiation facility through project no. EMIR 2019 18-7099. **Author contributions:** C.P., M.D.B., P.M., E.Z., and M.K. fabricated the microstructures. V.S., E.Z., P.M., and M.K. performed the electron irradiation. S.K. grew the single crystals. C.P. and P.J.W.M. performed the transport measurements and data analysis. C.P., T.O., R.M., A.S., A.P.M., and P.J.W.M. interpreted the data. All authors were involved in designing the experiment and writing the manuscript. **Competing interests:** The authors declare no competing interests. **Data and materials availability:** All experimental data in the main text and supplementary materials are available at Zenodo (33).

#### SUPPLEMENTARY MATERIALS

science.sciencemag.org/content/368/6496/1234/suppl/DC1  
Materials and Methods  
Supplementary Text  
Figs. S1 to S9  
Table S1  
References (34–37)

24 July 2019; accepted 22 April 2020  
10.1126/science.aay8413

## ***h/e* oscillations in interlayer transport of delafossites**

Carsten Putzke, Maja D. Bachmann, Philippa McGuinness, Elina Zhakina, Veronika Sunko, Marcin Konczykowski, Takashi Oka, Roderich Moessner, Ady Stern, Markus König, Seunghyun Khim, Andrew P. Mackenzie and Philip J.W. Moll

*Science* **368** (6496), 1234-1238.  
DOI: 10.1126/science.aay8413

### **Coherent electronic waves**

The wave nature of conducting electrons in solids can be revealed through interference effects. In layered materials, these effects are most often seen in in-plane transport. By contrast, Putzke *et al.* studied electronic transport perpendicular to the conductive layers in the ultraclean delafossites PdCoO<sub>2</sub> and PtCoO<sub>2</sub>. When an in-plane magnetic field was applied, the electrical resistance exhibited periodic oscillations as a function of field magnitude. The findings can be explained through a model that requires that the electronic waves remain coherent over macroscopic distances.

*Science*, this issue p. 1234

#### **ARTICLE TOOLS**

<http://science.sciencemag.org/content/368/6496/1234>

#### **SUPPLEMENTARY MATERIALS**

<http://science.sciencemag.org/content/suppl/2020/06/10/368.6496.1234.DC1>

#### **REFERENCES**

This article cites 36 articles, 4 of which you can access for free  
<http://science.sciencemag.org/content/368/6496/1234#BIBL>

#### **PERMISSIONS**

<http://www.sciencemag.org/help/reprints-and-permissions>

Use of this article is subject to the [Terms of Service](#)

---

*Science* (print ISSN 0036-8075; online ISSN 1095-9203) is published by the American Association for the Advancement of Science, 1200 New York Avenue NW, Washington, DC 20005. The title *Science* is a registered trademark of AAAS.

Copyright © 2020 The Authors, some rights reserved; exclusive licensee American Association for the Advancement of Science. No claim to original U.S. Government Works